

Boise State University
ScholarWorks

Electrical and Computer Engineering Faculty
Publications and Presentations

Department of Electrical and Computer
Engineering

1-24-2001

Estimating Scanning Characteristics from Corners in Bilevel Images

Elisa H. Barney Smith
Boise State University

Estimating scanning characteristics from corners in bilevel images

Elisa H. Barney Smith

Electrical and Computer Engineering Department
Boise State University, Boise, Idaho 83725, USA

ABSTRACT

Degradations that occur during scanning can cause errors in Optical Character Recognition (OCR). Scans made in bilevel mode (no grey scale) from high contrast source patterns are the input to the estimation processes. Two scanner system parameters are estimated from bilevel scans using models of the scanning process and bilevel source patterns. The scanner's point spread function (PSF) width and the binarization threshold are estimated by using corner features in the scanned images.

These estimation algorithms were tested in simulation and with scanned test patterns. The resulting estimates are close in value to what is expected based on grey-level analysis. The results of estimation are used to produce synthetically scanned characters that in most cases bear a strong resemblance to the characters scanned on the scanner at the same settings as the test pattern used for estimation.

Keywords: Image degradation, Point spread function, Intensity binarization, Scanner characterization, Synthetic character.

1. INTRODUCTION

With the advent of computers, the "paperless office" was imagined and promised to the world. What really developed was an increased production of paper documents and a need to have documents in both paper and electronic form. The conversion of paper documents into electronic form is done through electronic document scanners which produce a digital image. Sometimes this image is all that is needed, but often further processing and interpretation is desired. In either case, the bitmap of the document produced by the scanner is different from the source pattern that appears on paper. The spatial and intensity quantization that occurs during scanning changes the appearance of the image content such as characters and line drawings. Sometimes the digital image of a text document is converted into ASCII text files, possibly with formatting information, through optical character recognition (OCR), or schematics are converted to computer-aided design (CAD) files. The ability to characterize the degradations that are introduced in the conversion of the paper document into a digital binary image through the process of scanning is an important step towards improving processing accuracy.

Ho and Baird analyzed the effect that different model parameters have on OCR accuracy and determined that the two most significant parameters are PSF width and binarization threshold¹⁰. While many methods are available to estimate the scanner characteristics from a grey-level scan^{4-8, 13-16}, very little research has been completed on estimating scanner parameters from bilevel scans^{1,3}. The scanner calibration methods that use grey-level information either directly or indirectly consider the profile of the blurred edge. With bilevel images, the profile is no longer available, only the location of the edges. This requires new estimation techniques.

2. SCANNER MODEL

The basic scanner model describes the sampling of the spatially continuous image of "blackness" $o(x, y)$, where blackness is 1-reflectance. The values of $o(x, y)$ can vary from 0 (white) to 1 (black). The value of each pixel in the scanned image before intensity quantization, $s(i, j)$, depends on the reflectance in the original image in a neighborhood around the scanning sensor. The weighting of the contribution of the source reflectance to the sensor value is a function of the distance from the sensor center, called the *point spread function* (PSF), $PSF(x, y)$. In ideal sampling, the PSF will be an impulse function, but the real sensor receives light from an area of the paper. Further distortion can come from the optics of the scanning system or from charge in the photosensor migrating to a more distant sensor's potential well. Thus we model the

Correspondence: Email: EBarneySmith@boisestate.edu; Phone: 208-426-2214

signal, $s(i, j)$, that is received at each sensing element (i, j) as the convolution, or blurring, of the PSF with the original image, $o(x, y)$, sampled at points x_i, y_j on a rectangular grid^{9,11}.

$$s(i, j) = \iint PSF(x_i - u, y_j - v) \cdot o(u, v) du dv \quad (1)$$

This follows the common practice of assuming spatial-invariance over the field of view, which is valid for small regions.

To produce a bilevel image, as is most commonly used for text, the intensity is quantized by applying a *thresholding* operation:

$$f(i, j) = \begin{cases} 1 & s(i, j) \geq \Theta \\ 0 & s(i, j) < \Theta \end{cases} \quad (2)$$

A higher threshold value, Θ , reduces the number of black pixels in $f(i, j)$.

This whole process is combined in the diagram shown in Figure 1. The area within the dashed lines represents the scanner. In this research, methods to estimate the parameter of the PSF and the threshold are developed and tested.

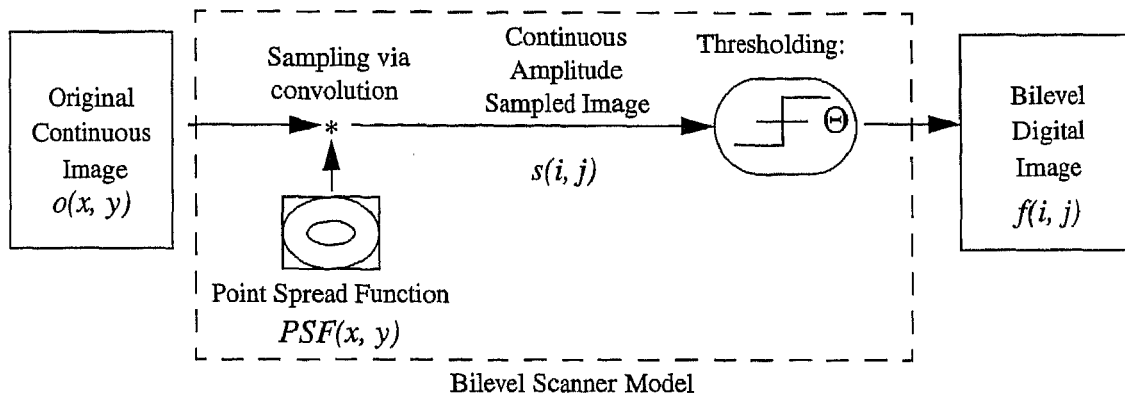


Figure 1: This scanner model is used to determine the value of the pixel (i, j) centered on each sensor element.

3. ESTIMATION OF PSF & THRESHOLD FROM WEDGES

In [2] the displacement of an edge was found as a function of PSF width and binarization threshold. This assumed edges were spaced far apart. Now information from where edges meet (corners) is used to estimate the PSF width and binarization threshold separately. This is advantageous because wedges, such as corners, should be plentiful in printed text and line drawings.

A wedge which has an angle measure of ϕ , as shown in Figure 2a,b, will no longer have a sharp corner after blurring (Figure 2c) and thresholding (Figure 2d). The displacement from the original edge location will be one of the configurations shown in Figure 3 depending on the scanner parameters. The original corner location will be unknown and cannot be used to decide which of the three cases in Figure 3 has occurred.

The most notable feature in a blurred and thresholded wedge is the rounded corner. The rounding of the corner, for a given angle ϕ , depends on the threshold (Θ) and PSF width (w). This can be quantified by the distance between points p_1 and p_2 in Figure 4, which is an enlarged view of Figure 3a. Measuring the distance between the extrapolated vertex point p_1 and the apex point p_2 , the erosion distance (d_1), will allow us to determine the threshold and the PSF width.

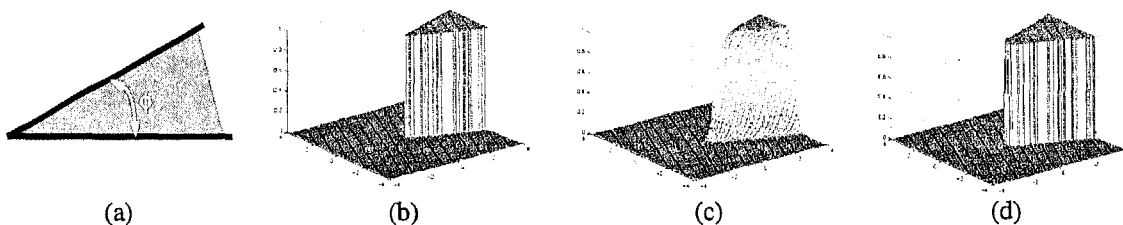


Figure 2: Illustration of a black wedge on a white background of angle ϕ before blurring and thresholding. (a) top view, (b) 3-D view (c) after blurring (d) after blurring and thresholding.

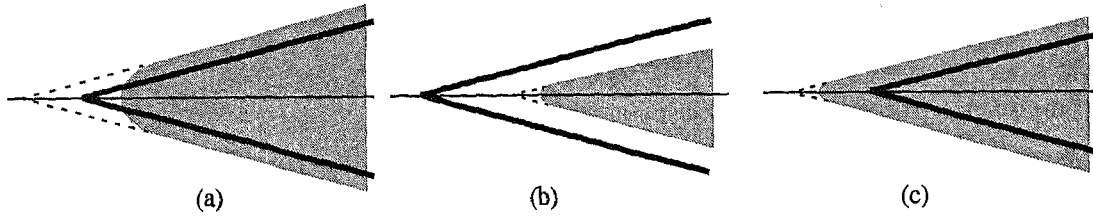


Figure 3: Three possible ways in which a blurred wedge (grey area) may be displaced from the original position (black lines).

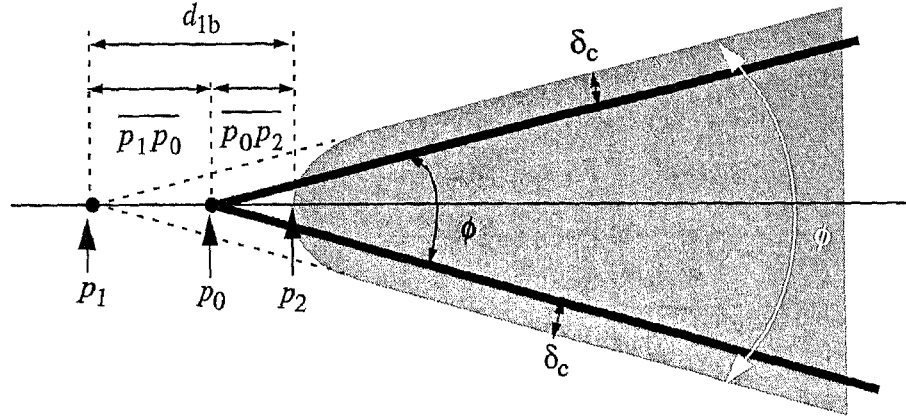


Figure 4: Magnification of corner (a) from Figure 3 showing measurements after blurring and thresholding.

Point p_0 is the location of the apex of the original wedge. Point p_1 is the point that would be at the intersection of the edges if they were extrapolated until they met. A line can be fitted to each edge and the location of point p_1 can be determined to subpixel accuracy. Point p_2 is the apex of the blurred and thresholded wedge. Points p_0 , p_1 and p_2 are collinear so the positions of features in the wedge after blurring and thresholding can be described analytically relative to the original wedge.

The distance between points p_0 and p_1 depends on the angle ϕ and the displacement of the edge, δ_c . The blurring and thresholding of the wedge will relocate the edges by the displacement δ_c , as described in [2], for parts of the edge sufficiently far from the tip of the original edge, point p_0 . This edge displacement is related to w and Θ by

$$\delta_c = -w \text{ESF}^{-1}(\Theta) . \quad (3)$$

The distance between interpolated wedge tip, point p_1 , to point p_0 can thus be written in terms of ϕ and δ_c :

$$\overline{p_1 p_0} = \frac{\delta_c}{\sin(\phi/2)} = \frac{-w \text{ESF}^{-1}(\Theta)}{\sin(\phi/2)} . \quad (4)$$

The scanned edges will be parallel to the original edges, allowing the angle ϕ to be measured.

The point p_2 is the point along the angle bisector where the blurred wedge equals the threshold value. The equation for the amplitude of the blurred wedge along its line of symmetry can be written as a function of w and ϕ ,

$$f_b(d_{0b}; w, \phi) = \int_{x=0}^{x=\infty} \int_{y=-x \tan \frac{\phi}{2}}^{y=x \tan \frac{\phi}{2}} \text{PSF}(x-d_{0b}, y; w) dy dx . \quad (5)$$

This is only integrable for certain PSF like the square pulse. For other PSF, it is calculated numerically. Figure 5 shows a plot of the profile of a wedge along its bisector for (a) three angles with a constant Gaussian PSF width, σ , and (b) three PSF widths for a constant angle ϕ . The distance that a wedge is eroded from the original apex point p_0 depends on the threshold and the profile of the blurred wedge

$$\overline{p_0 p_2} = f_b^{-1}(\Theta; w, \phi) . \quad (6)$$

The distance between points p_1 and p_2 is the sum of the two distances since the points are collinear, thus

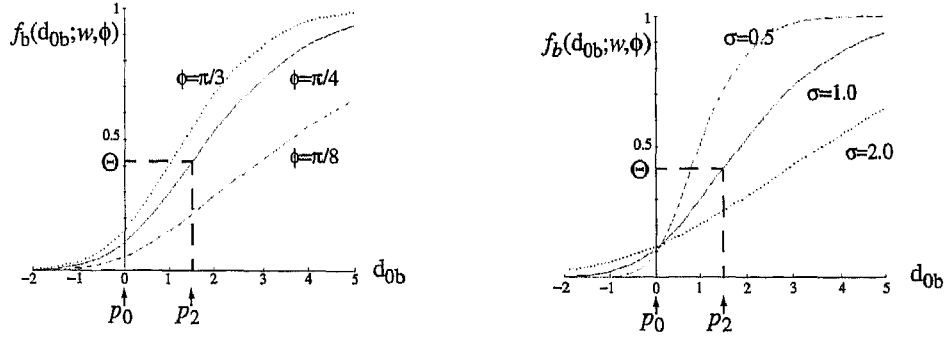


Figure 5: Plot of corner profile along bisector (a) Gaussian PSF width $\sigma=1$, and angles $\phi=\pi/3, \pi/4, \pi/8$ and (b) angle $\phi=\pi/4$ and Gaussian PSF widths $\sigma=0.5, 1, 2$.

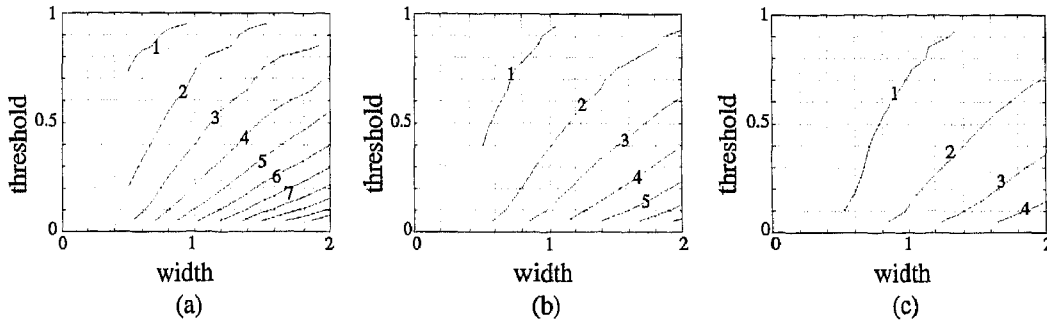


Figure 6: Observable erosion contours for constant d_{1b} iso-contours (a) $\phi=\pi/6$ (b) $\phi=\pi/4$ (c) $\phi=\pi/3$

$$d_{1b} = \overline{p_1 p_2} = \overline{p_1 p_0} + \overline{p_0 p_2} = \frac{-wESF^{-1}(\Theta)}{\sin(\phi/2)} + f_b^{-1}(\Theta; w, \phi) . \quad (7)$$

This observable erosion distance, d_{1b} , is a function of w , Θ and ϕ and can be measured from an image. The parameters w and Θ are unknown, and ϕ is the angle which can be measured from the image. For the other two cases in Figures 3b and 3c, the steps of the calculations are slightly different, but the formulation of the erosion distance, d_{1b} , will be the same as in Equation 7.

The value of d_{1b} can be calculated for a specific angle, ϕ , and several (w, Θ) values. When ϕ and d_{1b} are measured from an image, a locus of (w, Θ) points that could have produced these measurements can be found as contours on the d_{1b} surface as in Figure 6. Different angles produce contours of similar shape, but the distance between contours for d_{1b} measurements separated by 1 pixel depends on the angle.

To obtain a unique (w, Θ) pair, more data from a different observation is needed. Measurements using white wedges on black backgrounds produce counterparts to those for black wedges. Following a similar derivation, and noting that blurred white wedges are 1 minus the value of blurred black wedges, we obtain

$$d_{1w} = \frac{-wESF^{-1}(1-\Theta)}{\sin(\phi/2)} + f_b^{-1}(1-\Theta; w, \phi) . \quad (8)$$

It can be seen that the black and white contours are symmetric to each other about the $\Theta=1/2$ line.

This difference in orientation of constant erosion iso- d_{1b} and iso- d_{1w} curves for black and white wedges can be utilized for parameter estimation by scanning at least one black wedge and one white wedge. The intersection of the iso- d_1 contours from black and white wedges should be at the (w, Θ) value for that scanner (Figure 7). This method will still work when d_1 data is collected from black and white wedges of different angle measures, increasing the amount of data that can be used on a given page of text or in a given line drawing.

The estimate of the location of point p_2 , the apex of the scanned wedge, is restricted to an integer value. In theory, p_2 can be at any real-valued location. Thus p_2 , and also d_1 , will have an error in the range $[-0.5, 0.5]^{12}$. To get a better estimate of d_1 , several wedges at different offsets relative to the sampling grid are needed. Each wedge image produces an estimate of ϕ and d_1 . The d_1 estimates can not be directly averaged since ϕ may be different between wedges. Instead, the d_1 contour representing plausible (w, Θ) values are created for each ϕ, d_1 pair. The $N_{black} \times N_{white}$ intersection points at each threshold are

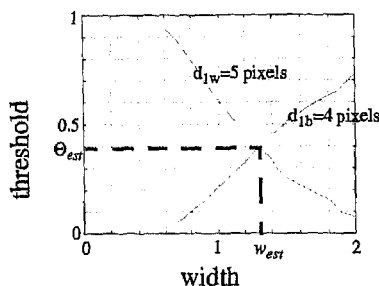


Figure 7: The system parameter estimate is where iso- d_{1b} and iso- d_{1w} contours intersect.

located and the mean of the intersection points is the final estimate which should be more accurate, on average, than any single point.

4. RESULTS

Three PSF assumptions (triangular pulse or cone, Gaussian and Cauchy) were used in estimation with isolated wedges. Two scanners were used, an HP Scanjet 4c (600dpi optical resolution) and an Apple Color One Scanner (300dpi optical resolution). Estimates were made at 17 reflectance thresholds.

Estimation experiments were run using wedges with angles measuring from 5° to 60° in 5° increments. To reduce the effects of printing in the comparison, the wedges were printed using the phototypesetter at a resolution of 80 dots per mm (2034 dpi). Each of these wedges were scanned five times, each with the chart at a different location on the scanning platen to give the wedges different phase offsets relative to the sensors. This gave $N_{black}=5$ black and $N_{white}=5$ white corners for each of 12 angles at each threshold.

Figure 8a shows erosion distance d_1 contours under Gaussian PSF assumption for wedges scanned by the HP scanner at a reflectance threshold of 0.31 and angle, $\phi=45^\circ$. There is one contour for each of the N_{black} black and each N_{white} white corners. These intersect at $N_{black} \times N_{white}$ points. The mean of these intersection points is the estimate for the PSF width and binarization threshold, which is shown with a large star. This process of estimating a contour for each scan of each wedge and averaging the intersection points for 5 black and 5 white wedges to find an estimate was repeated for the 11 other angles.

Figure 8b shows the mean of the estimates for the HP scanner at each of the 12 different angles at the reflectance threshold level 0.31. The estimates vary over a small region in the width, threshold space. These points were averaged to give the final estimation result for each threshold.

The process was repeated to obtain PSF width and binarization threshold estimates from the set of wedges at each of 17 thresholds on an HP and an Apple scanner. The average width and standard deviation of the estimated widths are shown in Table 1 for the HP scanner and in Table 2 for the Apple scanner. The width parameters estimated from a grey-scale knife edge on the same scanners are also shown in these tables. As the PSF was found to be anisotropic for both these scanners, a range of PSF widths are shown. The estimated reflectance $(1-\Theta)$ is compared with the reflectance threshold in Figure 9.

Using a process equivalent to that in Figure 1, the estimated (w, Θ) values were used to create synthetic characters shown in Tables 3 and 4. Phototypeset printed characters matching the input to the simulation were scanned at multiple thresholds matching the thresholds at which the wedges were scanned in estimation experiments. The triangular pulse, Gaussian and Cauchy PSF were used in parameter estimation and the synthetic characters produced under the three assumptions are

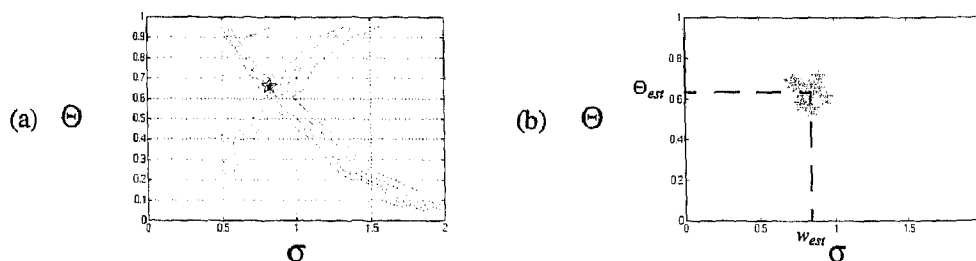


Figure 8: (a) Erosion distance d_1 contours from 5 black and 5 white $\phi=45^\circ$ wedges at a reflectance threshold of 0.31 scanned on the HP scanner. Contours are shown for three PSF Gaussian assumptions and (b) Mean estimates from 12 different angles are combined to get a final estimate.

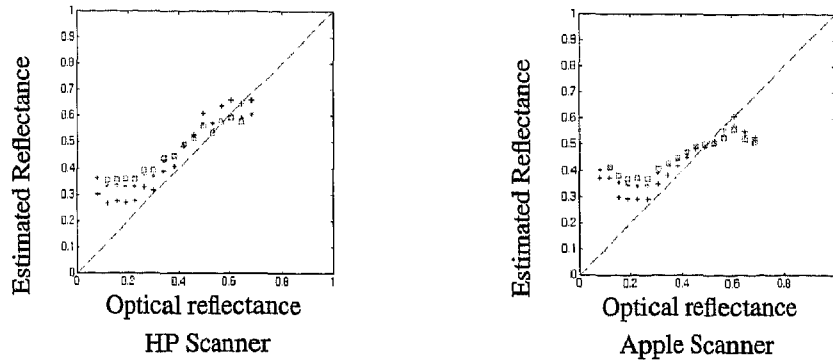


Figure 9: Comparison of estimated reflectance threshold ($1-\Theta$) from sector merge width versus reflectance associated with scanning threshold.

Table 1: PSF width estimation results summary using isolated wedge estimation on HP scanner

PSF	Mean Width Parameter Estimate	Standard Deviation	Number of Points (from 17)	Knife Edge Width Estimates
Triangular Pulse (w_T)	4.76	0.72	15	4.22 - 5.26
Gaussian (σ)	1.03	0.24	17	0.90 - 1.14
Cauchy (α)	0.72	0.16	17	0.50 - 0.65

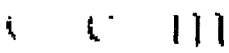







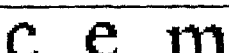

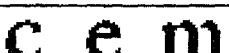





Table 2: PSF width estimation results summary using isolated wedge estimation on Apple scanner

PSF	Mean Width Parameter Estimate	Standard Deviation	Number of Points (from 17)	Knife Edge Width Estimates
Triangular Pulse (w_T)	4.38	0.71	16	3.56 - 5.65
Gaussian (σ)	0.94	0.27	17	0.77 - 1.22
Cauchy (α)	0.66	0.18	17	0.46 - 0.74

Table 3: Comparison of scanned and synthetic characters based on isolated wedges estimates. - HP scanner

Threshold	Scanned Characters	PSF		
		Triangular	Gaussian	Cauchy
0.15	c e m	cem	cem	cem
0.31	c e m	cem	cem	cem
0.50	c e m	cem	cem	cem
0.64	c e m	cem	cem	cem

Table 4: Comparison of scanned and synthetic characters based on isolated wedges estimates. - Apple scanner

Threshold	Scanned Characters	PSF		
		Triangular	Gaussian	Cauchy
0.15				
0.31				
0.50				
0.64				

shown for 4 representative thresholds.

5. DISCUSSION

This estimation method uses isolated wedges to estimate w and Θ . The PSF widths are within the range of values estimated using grey level methods. For mid-valued binarization thresholds the estimates are also very close. The estimates are dependent on the accuracy of the erosion database and the measurement of the erosion distance. The difficulty encountered in the creation of the erosion database is that both the Gaussian and Cauchy have an infinite support making it difficult to accurately calculate the blurred wedge numerically. The Gaussian PSF can be truncated at 3σ with minimum effect. The Cauchy will still be affected by truncation at any radius.

The w and Θ values depend on the measured erosion distance, d_1 . When the wedge angle is small, the noise in the wedge scan may cause the wedge to have multiple connected components. The small isolated fragments at the tip of the wedge are not considered part of the wedge in the current implementation and their omission changes the estimate of d_1 by several pixels. Larger angles are not as susceptible to breaking, but the contours from the erosion database are widely spaced for pairs of d_1 distances that differ by 1 pixel, thus an error of 1 pixel caused by noise on the apex pixel or phase effects will greatly affect the estimates for large angles. Angles with measurements between 15° and 40° produce the smallest variance in estimates.

The reflectance threshold estimates are closer to the actual reflectance or midranged reflectances, but do not reach the extreme reflectances. The extreme reflectance thresholds will produce the greatest breaking in small-angled wedges, which interferes with estimation. The threshold estimates at extreme thresholds were affected such that the threshold estimates were mostly between levels of 0.3 and 0.6. Some of the errors in estimates at very high and low thresholds are related to poor estimates of d_1 due to drop out at small angles. Anisotropy in the real PSF will also affect the estimates in this method. All the wedges were scanned with a horizontal principal axis. This will make the wedges appear narrower which will skew the estimates, mostly at the extreme thresholds.

The synthetic characters bear a resemblance to scanned characters, with this similarity being stronger at mid-ranged threshold, which is consistent with the above observations. At extreme thresholds, stroke width is a more visible feature than corner erosion. This is a point for future research. These synthetic characters could be used in training an OCR engine to improve accuracy. The scanning of a test chart containing several wedges at the beginning of a production run could be used to calibrate the system and tune the OCR.

Work on this topic will continue to extract wedges from character images and use these to form w and Θ estimates. If the width of the PSF or more likely the binarization threshold of the scanner were to change with time, character images could be used to monitor and adjust the OCR parameters during a batch. A page of characters would have large N_{black} and N_{white} values. Thus the best way to combine the N_{black} and N_{white} loci of w and Θ values will also be investigated.

ACKNOWLEDGEMENT

I would like to thank George Nagy for his useful ideas and comments that contributed to this work.

REFERENCES

1. Henry S. Baird, "Calibration of document image defect models," *Proc. of Second Annual Symposium on Document Analysis and Information Retrieval*, Las Vegas, Nevada, April 1993, pp. 1-16.
2. Elisa H. Barney Smith, "Characterization of Image Degradation Caused by Scanning," *Pattern Recognition Letters*, Volume 19, Number 13, 1998, pp. 1191-1197.
3. Elisa H. Barney Smith, *Optical Scanner Characterization Methods Using Bilevel Scans*, Doctoral Thesis, Rensselaer Polytechnic Institute, December, 1998.
4. M. Michael Chang, A. Murat Tekalp, A. Tanju Erdem, "Blur Identification using the Bispectrum," *IEEE Trans. Signal Processing*, Vol. 39, October 1991, pp. 2323-2325.
5. F. Chazallet, J. Glasser, "Theoretical bases and measurements of the MTF of integrated image sensors," *Proc. SPIE Image Quality: An Overview*, Vol. 549, Arlington, VA, 9-10 April 1985, pp. 131-144.
6. Luigi P. Cordella and George Nagy, "Quantitative Functional Characterization of an Image Digitization System," *6th International Conference on Pattern Recognition*, Munich, Germany, 19-22 October 1982, pp. 535-537.
7. D. B. Gennery, "Determination of Optical transfer function by inspection of the frequency domain plot," *Journal of the Optical Society of America*, Vol. 63, No. 12, December 1973, pp. 1571-1577.
8. C. A. Glasbey, G. W. Horgan, D. Hitchcock, "A note on the grey-scale response and sampling properties of a desktop scanner," *Pattern Recognition Letters*, Vol. 15, No. 7, 1994, pp. 705-711.
9. Rafael C. Gonzalez, Richard E. Woods, *Digital Image Processing*, Addison-Wesley Publishing Co., 1993.
10. Tin Kam Ho and Henry S. Baird, "Large-Scale Simulation Studies in Image Pattern Recognition," *IEEE Transactions on Pattern Analysis and Machine Intelligence*, Vol. 19, No. 10, October 1997, pp. 1067-1079.
11. A. K. Jain, *Fundamentals of Digital Image Processing*, Prentice Hall, Englewood Cliffs, NJ, 1989
12. Prateek Sarkar, George Nagy, Jiangying Zhou, Daniel Lopresti, "Spatial Sampling of Printed Patterns," *IEEE Transactions on Pattern Analysis and Machine Intelligence*, Vol. 20, No. 3, March 1998, pp. 344-351.
13. S. E. Reichenbach, S. K. Park, R. Narayanswamy, "Characterizing digital image acquisition devices," *Optical Engineering*, Vol. 30, No. 2, March 1991, pp. 170-177.
14. R. M. Simonds, "Two-dimensional modulation transfer functions of image scanning systems," *Applied Optics*, Vol. 20, No. 4, February 1981, pp. 619-622.
15. P. L. Smith, "New Technique for Estimating the MTF of an Imaging System from its Edge Response," *Applied Optics*, Vol. 11, No. 6, June 1972, pp. 1424-1425.
16. H. Wong, "Effect of knife-edge skew on modulation transfer function measurements of charged couple device imagers employing a scanning knife edge," *Optical Engineering*, Vol. 30, No. 9, 1991, pp. 1394-1398.